Metamagnetic Transition in EuSe₂: A New, Metastable Binary Rare-Earth Polychalcogenide

Jennifer A. Aitken,[†] Jerry A. Cowen,[‡] and Mercouri G. Kanatzidis*,[†]

Department of Chemistry and Department of Physics and Astronomy and Center for Fundamental Materials Research, Michigan State University, East Lansing, Michigan 48824-1322

The reaction of Eu with molten lithium polyselenide produced a new rare-earth dichalcogenide, $EuSe_2$. This compound cannot be obtained via direct combination of the elements and is therefore an example of how alkali metal chalcogenide fluxes can access metastable or kinetically stable phases. The crystals of $EuSe_2$ are very dark red and air stable for several months. The structure was determined with single-crystal X-ray diffraction. The compound crystallizes in the tetragonal space group, $I4/mcm$ (#140) with $a = 6.391(1)$ Å and $c = 7.848(1)$ Å, $Z = 4$, R1 = 3.9%, and wR2 = 10.0%. It adopts the $CuAl_2$ structure type, and contains rows of staggered diselenide dumbbells running parallel to the c-axis, separated by rows of square antiprismatically coordinated Eu atoms. $EuSe_2$ is a semiconductor with a band gap of 1.43 eV and decomposes at 569 °C to the more stable cubic EuSe. $EuSe_2$ displays metamagnetic behavior below 8 K. Variable temperature magnetic susceptibility and magnetization measurements were performed on single-crystal samples to study this phenomenon. A model is proposed in which all Eu spins in the ab-plane are coupled ferromagnetically, whereas alternate sheets are coupled antiferromagnetically to form a bulk antiferromagnet. The Se–Se bond stretch exhibits a Raman shift of 256 cm⁻¹.

Introduction

Recently, there has been a renewed interest in binary rare-earth chalcogenides. A review by Kumta and Risbud describes the rare-earth chalcogenides, binary and ternary, as an emerging class of optical materials.[1] In the past, high-temperature and high-pressure methods were used to synthesize these types of compounds, such as direct combination of the elements or treatment of H_2Q (Q = S, Se) on the rare-earth oxide or salt.[2] Recently, Parkin and Fitzmaurice have dissolved europium (Eu) and ytterbium (Yb) in liquid ammonia to prepare binary sulfides, selenides, and tellurides.[3] Also, Chen and Dorhout have recently reinvestigated the binary chalcogenides of lanthanum and praseodymium via moderate-temperature metathesis reactions using molten alkali metal polychalcogenide salts and lanthanide halides.[4]

Prior to our study, there were only two known binary phases containing Eu and selenium (Se), $EuSe$[5] (NaCl type[6]) and Eu_2Se_3[7] (Sc_2S_3 type[8]). To our knowledge, the only attempt to discover more binary phases containing

Eu and Se was in 1975, by Eliseev, Sadovskaya, and Van Tam.[7] However, this study was not very thorough and still there is no phase diagram available for the Eu/Se system.

Molten alkali metal polychalcogenide fluxes have been very successful in preparing new ternary and quaternary rare-earth chalcogenides.[9–14] In most cases, these salts act not only as solvents but also as reactants, providing species that can be incorporated into the final product. As the size of the alkali metal increases, the basicity increases as well as the probability that it will be incorporated into the final product. We can use this knowledge to our advantage. Often salts of sodium or lithium can be used to provide a good flux for the reaction, yet do not become incorporated into the final product. This is the case for $EuSe_2$, which was first found in the quaternary system Li/Eu/P/Se. This is not

---

* Author to whom correspondence should be sent.
† Department of Chemistry.
‡ Department of Physics and Astronomy.
(1) Kumta, P. N.; Risbud, S. H. *J. Mater. Sci.* **1994**, *29*, 1135.
(2) Guittard, M.; Flahaut, J. Synthesis of Lanthanide and Actinide Compounds; Meyer, G.; Morss, L. R., Eds.; Kluwer: Dordrecht, 1991; pp 321–347.
(3) Parkin, I. P.; Fitzmaurice, J. C. *Polyhedron* **1993**, *12*, 1569–1571.
(4) Chen, J. H.; Dorhout, P. K. *J. Solid State Chem.* **1995**, *117*, 318–322.
(5) Guittard, M.; Benacerrat, A. *C. R. Hebd. Seances de Acad. Sci.* **1959**, *248*, 2589–2591.

(6) Goldschmidt, V. M. *Skrifter Utgitt av det Norske Videnskaps-Akademi, Oslo* **1926**, *9*, 1.
(7) Eliseev, A. A.; Sadovskaya, O. S.; Van Tam, N. *Inorg. Mater., Translated From Izv. Akad. Nauk SSSR, Neorg. Mater.* **1975**, *11 (3)*, 361–364.
(8) White, J. G.; Dismukes, J. *Acta Crystallogr.* **1963**, *16*, 24.
(9) Kanatzidis, M. G.; Sutorik, A. C. *Prog. Inorg. Chem.* **1995**, *43*, 151–265.
(10) Sutorik, A. C.; Kanatzidis, M. G. *Chem. Mater.* **1997**, *9*, 387–398.
(11) Sutorik, A. C.; Albritton-Thomas, J.; Kannewurf, C. R.; Kanatzidis, M. G. *J. Am. Chem. Soc.* **1994**, *116*, 7706–7713.
(12) Sutorik, A. C.; Albritton-Thomas, J.; Hogan, T.; Kannewurf, C. R.; Kanatzidis, M. G. *Chem. Mater.* **1996**, *8 (3)*, 751–761.
(13) (a) Chen, J. H.; Dorhout, P. K.; Ostenson, J. E. *Inorg. Chem.* **1996**, *35*, 5627–5633. (b) Chondroudis, K.; McCarthy, T. J.; Kanatzidis, M. G. *Inorg. Chem.* **1996**, *35*, 840–844.
(14) (a) Cody, J. A.; Mansuetto, M. F.; Pell, M. A.; Chien, S.; Ibers, J. A. *J. Alloys Compd.* **1995**, *219*, 59–62. (b) Cody J. A.; Ibers, J. A. *Inorg. Chem.* **1995**, *34*, 3165–3172.

the first time that the molten salt technique produced a new binary chalcogenide from a quaternary system. For example, $BaTe_2$[15] which is, coincidentally, isostructural with $EuSe_2$, was discovered from the system Na/Ba/Ta/Te. Later, we devised a rational synthesis for preparing $EuSe_2$ using a Li_2Se_x flux. $EuSe_2$ cannot be formed via direct combination of the elements and is therefore a fine example of how molten salt synthesis can access metastable, or kinetically stable, phases rather than the thermodynamically stable ones.[9] Here we describe the synthesis, structure, and Raman spectrum, as well as the thermal and optical absorption properties of $EuSe_2$. We also investigated the magnetic properties of this material and discovered a well-defined metamagnetic transition below 8 K. To understand this unusual transition better, we performed in-depth measurements, on single crystals of $EuSe_2$, of the magnetic susceptibility as a function of orientation, magnetic field, and temperature. We propose a tentative magnetic model responsible for the observed behavior.

Experimental Section

Reagents. The chemicals in this work were used as obtained: (i) europium powder 99.9% purity, <250 μm, Alfa Aesar, Ward Hill, MA; (ii) selenium powder 99.5+%, 100 mesh, Aldrich Chemical Company, Inc., Milwaukee, WI; (iii) lithium metal rods, 99.9%, 12.7 mm diameter, Aldrich Chemical Co.; (iv) methyl alcohol 99.8+%, A. C. S. reagent, Aldrich Chemical Co.; and (v) diethyl ether, ACS Grade, anhydrous, Columbus Chemical Industries, Inc., Columbus, WI.

Synthesis of Li₂Se. Li_2Se was prepared by a modified literature procedure.[16] In an argon-filled drybox, 24.058 g (0.305 mol) of Se was combined with 4.229 g (0.610 mol) of freshly cut lithium metal and placed in a 1000-mL round-bottomed flask containing a Teflon-coated stir bar. This procedure was done under an atmosphere of argon instead of nitrogen because lithium reacts readily with nitrogen to form a lithium nitride. Liquid ammonia was condensed into the flask at −78 °C (dry ice/acetone bath) under argon, until the flask was two-thirds full, to give a dark blue/bronze colored solution. The solution was stirred for 1 day and then the ammonia was evaporated as the bath was warmed to room temperature. The light peach solid (almost 100% yield) was dried under vacuum overnight and ground to a fine powder with a mortar and pestle under a dry nitrogen atmosphere in a Vacuum Atmospheres Dri-Lab glovebox.

Preparation of EuSe₂. In a nitrogen-filled glovebox, 0.046 g (0.3 mmol) of Eu powder, 0.028 g (0.3 mmol) of Li_2Se, and 0.190 g (2.4 mmol) of Se were loaded into a graphite tube. The graphite tube was then placed into a 13-mm quartz tube and flame-sealed under vacuum (approximately 2×10^{-4} mbar). The tube was inserted into a programmable furnace and heated from 50 to 540 °C in 24 h. It was kept at 540 °C for 96 h. Finally, the temperature was decreased at a rate of 2 °C/h to 50 °C. The product was isolated by washing away the alkali chalcogenide flux with methanol and washing with ether. Dark red/black, rectangular brick-like crystals and cube-shaped, lighter red crystals were obtained (60/40% yield). Semiquantitative energy dispersive analysis (EDS) using a scanning electron microscope (SEM) on a number of the rectangular brick-like crystals gave an average composition of $EuSe_{2.33}$. The average composition of the cube-shaped crystals was $EuSe_{1.1}$. The crystals were easy to separate. The powder X-ray diffraction pattern of the cube-shaped crystals was indexed to the cubic phase, EuSe. The powder diffraction pattern of the

Table 1. Calculated and Observed X-ray Powder Diffraction Data of EuSe₂

hkl	d_{calc} (Å)	d_{obs} (Å)	I/I_{max}(obs) (%)[a]
110	4.5192	4.5101	6.39
002	3.9240	3.9178	4.14
200	3.1956	3.1906	7.82
112	2.9629	2.9587	100.00
211	2.6856	2.6815	22.56
202	2.4779	2.4737	20.48
220	2.2596	2.2547	4.49
310	2.0210	2.0167	12.42
222	1.9581	1.9573	17.02
213	1.9297	1.9265	12.35
312	1.7967	1.7962	3.73
321	1.7290	1.7267	3.10
024	1.6720	1.6685	4.90
402	1.4798	1.4772	7.52
323	1.4674	1.4658	2.46
420	1.4291	1.4284	1.61
332	1.4063	1.4044	12.60
215	1.3758	1.3731	4.04
422	1.3428	1.3418	1.70
116	1.2564	1.2556	3.58
150	1.2534	1.2521	3.58
206	1.2105	1.2095	1.50
521	1.1735	1.1725	2.11
424	1.1551	1.1537	1.97
440	1.1298	1.1277	1.39
352	1.0557	1.0544	2.57
127	1.0437	1.0417	1.79
406	1.0121	1.0108	2.52

[a] Only peaks with I/I_{max}(obs) >1% are listed.

rectangular blocks indicated a new phase. The same reaction was also conducted at 750 °C and gave the same result.

Physical Measurements. *Powder X-ray Diffraction.* Analyses were performed using a calibrated Rigaku-Denki/RW400F2 (Rotaflex) rotating anode powder diffractometer controlled by an IBM computer, operating at 45 KV/100 mA and with a 2°/min scan rate, employing Ni-filtered Cu radiation in a Bragg−Brentano geometry. Powder patterns were calculated with the Cerius2 software package.[17] A comparison of the observed and calculated powder diffraction data is listed in Table 1.

Electron Microscopy. Quantitative microprobe analyses of the compounds were performed with a JEOL JSM-35C Scanning Electron Microscope (SEM) equipped with a Tracor Northern Energy Dispersive Spectroscopy (EDS) detector. Data were acquired with an accelerating voltage of 20 kV and a 40 s accumulation time.

Differential Thermal Analysis (DTA). Differential thermal analysis (DTA) was performed with a computer-controlled Shimadzu DTA-50 thermal analyzer. Six single crystals weighing 23 mg were sealed in a carbon coated quartz ampule under vacuum. A quartz ampule containing alumina of equal mass was sealed and placed on the reference side of the detector. The sample was heated to 900 °C at 10 °C/min, kept there for 5 min, and then cooled at a rate of 10 °C/min to 100 °C, followed by rapid cooling to room temperature.

Solid-State UV/Vis/Near-IR Spectroscopy. Optical diffuse reflectance measurements were performed at room temperature using a Shimadzu UV-3101PC double-beam, double-monochromator spectrophotometer. The instrument is equipped with an integrating sphere and controlled by a personal computer. $BaSO_4$ was used as a 100% reflectance standard. The sample was prepared by grinding the crystals to a powder and spreading the powder on a compacted surface of the powdered standard material that had been preloaded into a sample holder. The reflectance versus wavelength data generated were used to estimate the band gap of the material by converting reflectance to absorption data.[18]

(15) Li, J.; Guo, H. *J. Solid State Chem.* **1995**, *117*, 247−255.

(16) Feher, F. *Handbuch der Präparativen Anorganischen Chemie*: Brauer, G., Ed.; Ferdinand Enke: Stuttgart, Germany, 1954; pp 280−281.

(17) CERIUS², Version 2.0, Molecular Simulations Inc., Cambridge, England, 1995.

Raman Spectroscopy. Raman spectra (600−175 cm^{-1}, at 4 cm^{-1} resolution) were recorded on a BIO-RAD FT Raman spectrometer equipped with a Spectra-Physics Topaz T10−106c 1.064 nm YAG laser and a GE detector. Single crystals were loaded into a glass tube.

Magnetic Measurements. Magnetization measurements as a function of applied magnetic field, temperature, and angle were made on a MPMS Quantum Design SQUID susceptometer in the temperature range of 2.5 to 300 K and magnetic fields of 0 to ±55 kG. The angle dependence was measured using a QD rotor that was programmed to measure from 0 to 180° in increments of 10°. The samples consisted of a few (5 or 6) large single crystals, approximately 1 to 2 mm in the longest dimension, with a total mass between 8 and 14 mg. The crystals were cemented to a quartz plate or to the rotor using superglue, which was easily removed later using acetone. The temperature-dependent magnetization was measured by first cooling the sample in zero field, turning on the measuring field (always 100 G), and measuring in increasing temperature—this is a zero field cooled (ZFC) measurement. The sample was then cooled in the measuring field and the measurement was repeated—this is a field cooled (FC) measurement. The field-dependent magnetization was measured at 2.5 K in a field sequence 0 to 55 to −55 to 55 kG, with the field parallel to the two principal axes. The angle-dependent magnetization was measured at several temperatures in a measuring field of 100 G. The results were corrected for core atom diamagnetism.

Single-Crystal X-ray Crystallography. A crystal with dimensions 0.18 × 0.22 × 0.10 mm was mounted on a glass fiber. A Siemens SMART Platform CCD diffractometer, operating at 50 KV/40 mA and using graphite monochromatized Mo Kα radiation, was used for data collection. No initial cell is needed to collect data by this procedure. The data collection technique is known as hemisphere collection. Here, a region of reciprocal space was surveyed to the extent of 1.3 hemispheres to a resolution of 0.75 Å. Three major swaths of frames were collected with 0.30° steps in ω and an exposure time of 20 s per frame, giving a total measurement time of <10 h. An initial cell was obtained using the SMART program.[19] The SMART program was used to extract reflections from 300 frames of the actual data collection. From the reflections extracted, the strongest 80 were used to find an initial unit cell. This cell was used to integrate the data using the SAINT program.[19] The final cell constants were determined from a set of 746 strong reflections obtained from data collection.

The empirical absorption correction was done using SADABS[20a] and all refinements were done using the SHELXTL[20b] package of crystallographic programs. Systematic absence conditions of the data set gave two possible acentric space groups, *I*4*cm* (#108) and $\bar{I}4c2$ (#120) and one centrosymmetric space group, *I*4/*mcm* (#140). The structure could only be solved in the space group *I*4/*mcm*. One Eu atom was found in the special position 4a (0, 0, 1/4) and one Se atom was found in the special position 8h (−x, −x + 1/2, 0). Both atoms were refined anisotropically to obtain an acceptable R1/wR2 of 3.9/10%. The calculations were performed on a Silicon Graphics Iris Indigo workstation. Refer to Table 2 for a complete summary of crystallographic data. See Tables 3 and 4 for positional parameters, isotropic and anisotropic temperature factors, and selected bond distances and angles.

(18) (a) Wendlandt, W. W.; Hecht, H. G. *Reflectance Spectroscopy*; Interscience: New York, 1966. (b) Kotüm, G. *Reflectance Spectroscopy*; Springer-Verlag: New York, 1969. (c) Tandon, S. P.; Gupta, J. P. *Phys. Status Solidi* **1970**, *38*, 363−367.

(19) SMART and SAINT. Data Collection and Processing Software for the SMART System. Siemens Analytical X-ray Instruments Inc., 1995.

(20) (a) Sheldrick, G. M. University of Göttingen, Germany, to be published. (b) SHELXTL V-5, Siemens Analytical X-ray Systems Inc., Madison, WI 53719.

Table 2. Crystallographic Data for EuSe$_2$

parameter	data
crystal data	
formula weight	309.88
F(000)	524.00
crystal system	tetragonal
a, Å	6.391(1)
c, Å	7.848(1)
volume, Å^3	320.56(8)
Z	4
space group	I4/*mcm* (#140)
density (calculated), g/cm^3	6.420
absorption coefficient, mm^{-1}	41.951
data collection	
wavelength (Mo Kα), Å	0.71073
temperature, K	173.1
θ_{max} for data collection, deg.	27.02
index ranges	−8 ≤ *h* ≤ 7
	−8 ≤ *k* ≤ 4
	−10 ≤ l ≤ 9
reflections collected	872
independent reflections	110 [R(int) = 0.0501]
solution and refinement	
solution	direct methods
refinement method	full-matrix least-squares on F^2
max and min transmission	0.087015 and 0.034906
data/restraints/parameters	110/0/8
goodness-of-fit on F^2	1.511
final R indices [*I*.2 σ (*I*)]	R1 = 3.85%, wR2 = 9.97%
R indices (all data)	R1 = 3.87%, wR2 = 9.98%
extinction coefficient	0.0001(1)
largest diff peak and hole, e$^-$/Å^3	1.183 and −2.744

^{a} R1 = $\sum ||F_o| - |F_c||/\sum|F_o|$; wR2 = $\{\sum[w(F_o^2 - F_c^2)^2]/\sum[w(F_o^2)^2]\}^{1/2}$

Table 3. Fractional Atomic Coordinates and Anisotropic Displacement Parameters (Å^2 × 10^3) for EuSe$_2$

atom	*x*	*y*	*z*	$U_{eq}{}^a$
Eu	0.0000	0.0000	0.2500	9(1)
Se	0.3674(2)	0.1326(2)	0.0000	10(1)

atom	*U*11	*U*22	*U*33	*U*23	*U*13	*U*12
Eu	11(1)	11(1)	5(1)	0	0	0
Se	10(1)	10(1)	9(1)	0	0	1(1)

^{a} *U*(eq) is defined as one-third the trace of the orthogonalized U_{ij} tensor. The anisotropic displacement factor exponent takes the following form: $-2\pi^2[h^2a^2U_{11} + ... + 2hka^*b^* U_{12}]$.

Table 4. Selected Distances (Å) and Angles (deg) for EuSe$_2$

bonds		non-bonds	
Eu−Se × 8	3.1751(7)	Eu−Eu × 2	3.9240(6)
		Eu−Eu × 4	4.519(7)
Se−Se	2.397(4)	Se−Se	3.531(1)

Angles			
Eu−Eu−Eu	180.0		
Eu−Eu−Se	128.16(1)	Eu−Eu−Se	51.83(1)
Se−Eu−Se	84.62(5)	Se−Eu−Se	89.26(2)
Se−Eu−Se	67.55(1)	Se−Eu−Se	149.04(6)
Se−Eu−Se	140.95(6)	Se−Eu−Se	103.67(2)
Eu−Se−Eu	76.33(2)	Eu−Se−Eu	90.74(2)
Eu−Se−Eu	140.96(6)		
Eu−Se−Se	109.52(3)		

Results and Discussion

Synthesis and Thermal Analysis. EuSe$_2$ was first discovered in a quaternary chalcogenide system reaction. Later, rational reactions were designed to produce EuSe$_2$ in 60% yield by reacting Eu, Li$_2$Se, and Se in a 1:1:8 ratio at 540 °C. This reaction produces well-formed crystals with a typical size of 0.5 × 0.25 × 0.25
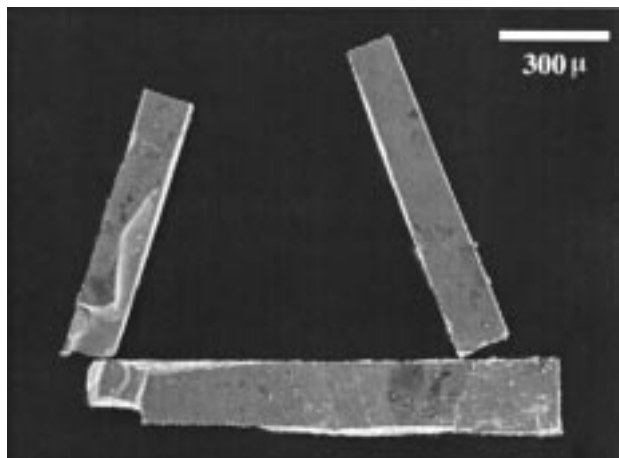
Figure 1. Scanning electron microscope photograph of flux-grown $EuSe_2$ crystals taken with an accelerating voltage of 20 kV.
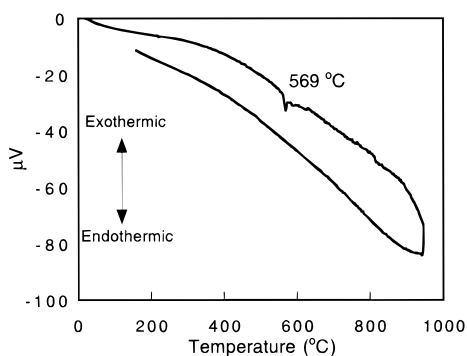
Figure 2. DTA diagram of $EuSe_2$. The irreversible decomposition to EuSe is indicated by the endothermic peak (heating rate: 10°/min).

mm, which can be seen in the SEM photograph shown in Figure 1. However, some crystals even reach 4 mm in the longest dimension. Direct combination of the elements at 500 or 900 °C does not produce $EuSe_2$, but rather EuSe and Se. Also, the reaction of Eu and Se in a 1:3 ratio gives the same result. Therefore, the flux uniquely enables the formation and crystal growth of the metastable phase rather than the more thermodynamically stable EuSe phase.

EuSe₂ seems to be relatively air stable for several months, but its thermal stability is not very high, as shown by the DTA spectrum in Figure 2. The compound does not melt congruently, decomposing endothermically at about 569 °C to produce EuSe and Se (see eq 1). This decomposition occurs because of the kinetically stable nature of $EuSe_2$ and the high thermal stability of the NaCl type structure.

$$EuSe_2 \rightarrow EuSe + Se \qquad (1)$$

The decomposition temperature of $EuSe_2$ is not inconsistent with the fact that the compound can be made at 750 °C in a Li_2Se_x flux because in these conditions the left-hand side of the equilibrium in eq 1 is favored.

After conducting extensive investigations in this area,[9,21] we have learned that polychalcogenide solids (i.e., compounds that contain chalcogen-chalcogen bonds) often cannot be prepared by high-temperature, direct-

combination techniques even in an excess of chalcogen, partly because of the thermal instability of the Q_x^{2-} (Q = S, Se, or Te) fragments. The instability increases with increasing x, resulting in smaller fragments as follows:[21]

$$Q_x^{2-} \rightarrow Q_{x-n}^{2-} + nQ \qquad (2)$$
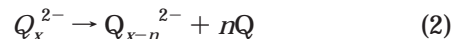
In molten A_2Q_x, polychalcogenide chain fragments of various lengths are formed. The internal chalcogen atoms can be considered to be neutral, whereas the terminal atoms bear the negative charge. The internal chalcogen atoms are oxidizing toward metals while they become reduced, breaking the Q_x^{2-} chains into smaller and smaller fragments. In the reaction to make $EuSe_2$, the $Se_{\sim 9}^{2-}$ chains break apart as they oxidize the Eu metal atoms. The latter then coordinate to the Se_2^{2-} fragments.

Structure. Europium is not exactly the typical lanthanide metal. Other lanthanides usually prefer a +3 oxidation state, whereas Eu would rather bear a +2 charge due to the exceptional stability of the half-filled f shell. Only four of the lanthanides, samarium, europium, thulium, and ytterbium, can have both valence states, +2 and +3. The stability of the divalent state is in the order[2] $Eu^{2+} > Sm^{2+} > Yb^{2+} > Tm^{2+}$. With this in mind we tried some reactions with samarium, but we did not find a new phase, instead we made beautiful crystals of the already known $SmSe_2$,[22] (Cu_2Sb type[23]) where samarium is in a trivalent state. In the case of Eu, the stability of the divalent state is large enough to deeply change the chemical, structural, and thermal behavior of its chalcogenides. The conditions of formation of EuS and EuSe are extremely different from those of the other rare-earth chalcogenides.[2]

Europium is very similar in size to the alkaline-earth metals. The ionic radius of Eu is 1.17 Å, whereas the ionic radii of calcium, strontium, and barium are 1.00, 1.18, and 1.35 Å respectively.[24] In addition to the oxidation state and ionic radius, Eu is also similar to the alkaline-earth metals in its general chemical reactivity. Europium, like alkali- and alkaline-earth metals, dissolves readily in liquid ammonia.[25–28] Also, divalent Eu compounds, such as europium sulfate, carbonate, and the halides, are isostructural with the strontium analogues and have very similar lattice parameters. With all these similarities between Europium and the alkaline earths it is not surprising that $EuSe_2$ adopts the same structure as that of SrS_2[29] and $BaTe_2$ ($CuAl_2$ type[30]). One major difference in these compounds is that whereas $EuSe_2$ is relatively air stable, SrS_2 and $BaTe_2$ are both air sensitive. The synthesis and struc-

(21) Kanatzidis, M. G. *Chem. Mater.* **1990**, *2 (4)*, 353–363.

(22) Eliseev, A. A.; Yarembash, E. I. *Inorg. Mater., Translated from Izv. Akad. Nauk SSSR, Neorg. Mater.* **1966**, *2 (8)*, 1167–1170.
(23) Elander, M.; Hägg, G.; Westgren, A. *Arkiv för Kemi, Mineralogi och Geologi* **1935**, *12B*, 1.
(24) Shannon, R. D. *Acta Crystallogr.* **1976**, *A32*, 751–767.
(25) Warf, J. C.; Korst, W. L. *J. Phys. Chem.* **1956**, *60*, 1590–1591.
(26) Thompson, D. S.; Schaefer, D. W.; Waugh, J. S. *Inorg. Chem.* **1966**, *5*, 325–326.
(27) Lagowski, J. J.; G. A. Moczygemba *The Chemistry of Non-Aqueous Solvents*, Academic Press: New York, 1967.
(28) Fishel, N. A.; Haschke, J. M.; Eick, H. A. *Inorg. Chem.* **1970**, *9*, 413–414.
(29) Kawada, I.; Kato, K.; Yamaoka, S. *Acta Crystallogr.* **1976**, *B32*, 3110–3111.
(30) Havinga, E. E.; Damsma, H.; Hokkeling, P. *J. Less-Common Met.* **1972**, *27*, 169.

KCeSe₄

EuSe₂

KCeSe₄
P 4/*nbm*
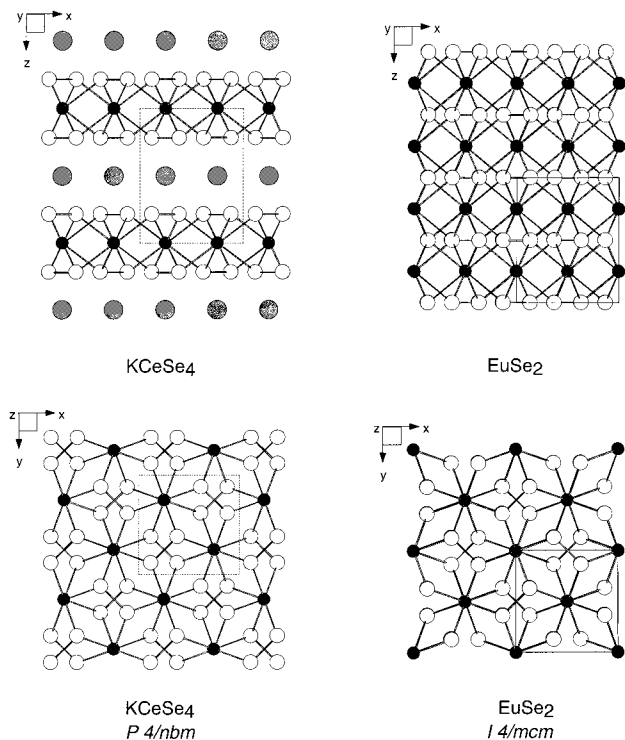
EuSe₂
I 4/*mcm*

Figure 3. Comparison of the structures of $KCeSe_4$ and $EuSe_2$ seen from two different directions, highlighting the relationship of the two compounds. The potassium, cerium/europium, and selenium atoms are shaded, black and white, respectively.

ture of these two compounds have been reported, but not any other types of characterization.

$EuSe_2$ is a very simple three-dimensional, Zintl-type compound. Looking down the *b*-axis, in the top right-hand corner of Figure 3, one can see the layers of Se stitched together by eight coordinate Eu atoms. Looking down the *c*-axis in Figure 4, one can see rows of diselenide dumbbells. These rows are packed together in a staggered fashion and run parallel to the *c*-axis, separated by rows of Eu atoms. Each Eu atom is bonded to eight Se atoms, with a distance of 3.1751(7) Å, and is in a square antiprismatic coordination. Every Eu atom is 3.9240(6) Å from two other Eu atoms in the *ac*-plane, and 4.519(7) Å from four other Eu atoms in the *ab*-plane. The bonding environment of a single Se atom can be described as a distorted square pyramid. The diselenide dumbbell sits inside of a rectangular, parallelepiped pocket, shown in Figure 5. Each Se atom is bonded to four Eu atoms and one other Se atom to make a diselenide unit with a Se−Se bond distance of 2.397(6) Å. This distance is comparable to the Se−Se bond distance in $KCeSe_4$, which is 2.385(3) Å.

The structure of $EuSe_2$ is closely related to that of $KCeSe_4$, which is also tetragonal and has dimensions similar to that of $EuSe_2$; that is, $a = 6.376(2)$ Å and $c = 8.327(1)$ Å.[10] As one can see from Figure 3, $KCeSe_4$ is a layered structure, where the anionic layers of $[CeSe_4]^-$ are separated by potassium ions. The $[CeSe_4]^-$ layers can be better expressed as $[Ce^{3+}(Se_2{}^{2-})_2]^-$. Because K and Ce have the same coordination environment, $KCeSe_4$ can be viewed as a derivative of the $CuAl_2$ structure type where the two cations alternate in the Cu positions along the *c*-axis. The space group for $KCeSe_4$ is $P4/nbm$, which is a subgroup of the space group $I4/mcm$.
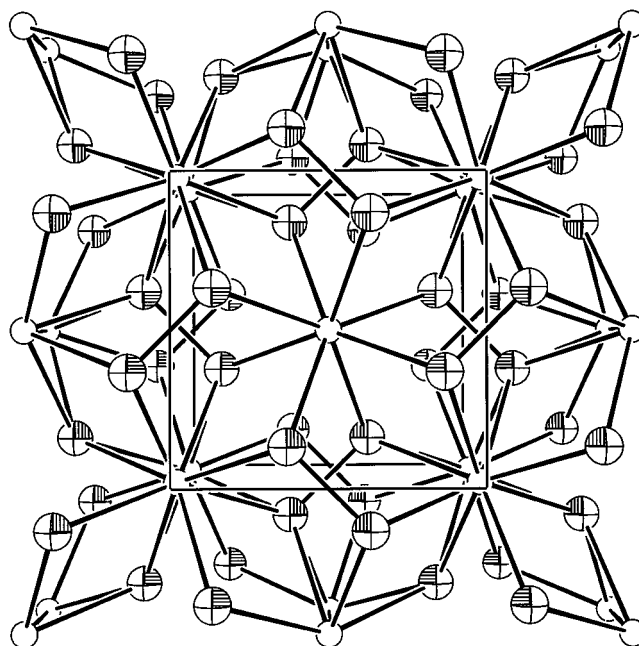
Figure 4. A projection of $EuSe_2$ viewed down the *c*-axis with thermal vibrational (90%) elipsoids. Rows of mutually perpendicular $Se_2{}^{2-}$ units are packed together in a staggered fashion and run parallel to the *c*-axis, separated by rows of Eu atoms. The $Se_2{}^{2-}$ units are stitched together by eight-coordinate Eu atoms in a square antiprismatic fashion. The Se atoms are shaded.
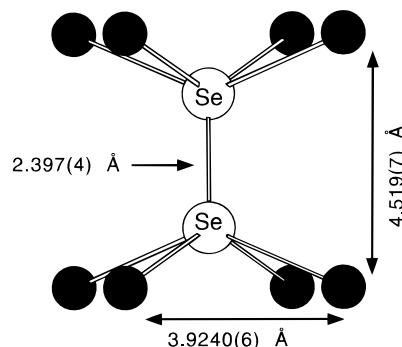
Figure 5. The immediate bonding environment of a diselenide dumbbell in $EuSe_2$ situated in a square-prismatic pocket.

$EuSe_2$ is not very much related to other binary lanthanide chalcogenides. Although every lanthanide, with the exception of terbium, has a chemical formula of $LnSe_2$, only $EuSe_2$ can be expressed as Ln^{2+} $Se_2{}^{2-}$. Among the other $LnSe_2$ compounds, there are only two structure types, they are, the $CeSe_2$ type[31] (which is basically the same as CeS_2[32]) and the Cu_2Sb type. The $CeSe_2$ type is found for cerium, praseodymium, and neodymium. In the structure there are two layers of $[LnSe]^+$ for every layer of $Se_2{}^{2-}$. All the lanthanides (except Eu and terbium) have $LnSe_2$ compounds of the Cu_2Sb type. This structure is closely related to $CeSe_2$, but there are no recognizable Se−Se bonds. The distance between the Se atoms in the square chalcogen net, of the ideal structure, is about 2.8 Å, however, it is

(31) Marcon, J. P.; Pascard, R. *Rev. Int. Hautes Temp. et des Refract., Paris* **1968**, *5*, 51.
(32) (a) Marsh, R. E.; Herbstein, F. H. *Acta Crystallogr.* **1983**, *39B*, 280−287. (b) Yanagisawa, Y.; Kanamaru, F.; Kume, S. *Acta Crystallogr.* **1979**, *35B*, 137−139.
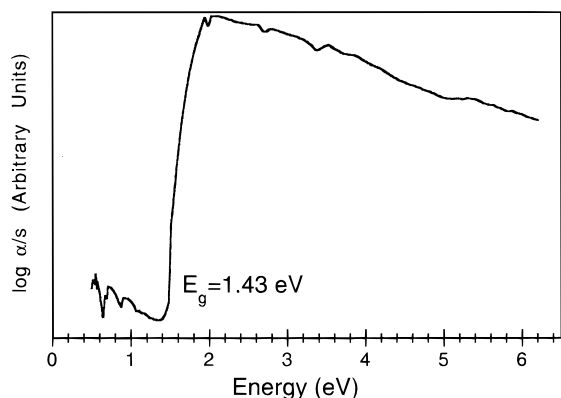
Figure 6. Optical absorption spectrum of EuSe₂.

known that a number of superstructures exist in these compounds that produce Se–Se bonds.[33]

Spectroscopy. The optical absorption properties of EuSe₂ were evaluated by examining the solid-state UV–vis diffuse reflectance spectrum. The spectrum in Figure 6 shows that EuSe₂ is a semiconductor, with a well-defined energy gap, E_g, of 1.43 eV. This value is optimum for absorption of solar energy and suggests its potential for photovoltaic and/or photoelectrochemical cells.

The Raman data are in good agreement with the structure. There is a single sharp peak at about 256 cm⁻¹ corresponding to the Se–Se stretching mode. This value is typical for the Se–Se stretching frequency.[34]

Magnetic Properties. Interest in the magnetic properties of divalent Eu compounds began ca. 1960 with the discovery, by Matthias, Bozorth, and VanVleck, that EuO was purely ferromagnetic with a Curie temperature of 77 K.[35] This discovery caused a number of research groups to investigate other similar divalent Eu compounds; for examples, EuS, EuSe, and EuTe.[36–38] All of these compounds have a cubic, NaCl type structure, which made them ideal for experimental and theoretical study. Although EuS and EuSe were found to be ferromagnetic, EuTe was found to exhibit antiferromagnetic coupling. Today, EuO and EuS are listed in the *CRC Handbook of Chemistry and Physics* in a table of selected ferromagnetic compounds.[39] With this in mind, we carefully investigated the magnetic behavior of EuSe₂. These experiments proved to be worthwhile because the magnetic behavior of EuSe₂ is interesting and unusual.

Initially, polycrystalline powder samples were examined with respect to variable-temperature molar magnetic susceptibility and field-dependent magnetization. The reciprocal molar susceptibility at high temperatures (50 to 300 K), shown in Figure 7A, clearly showed Curie–Weiss behavior with $\Theta = 14 \pm 2$ K and the Curie constant $C = 7.4 \pm 0.3$. From C we obtain a $\mu_{eff} = 7.7$

(33) Lee, S.; Foran, B. *J. Am. Chem. Soc.* **1994**, *116*, 154−161.
(34) Böttcher, P.; Getzschmann, J.; Keller, R. *Z. Anorg. Allg. Chem.* **1993**, 619, 476−488.
(35) Matthias, R. M.; Bozorth, R. M.; Van Vleck, J. H. *Phys. Rev. Lett.* **1961**, *7*, 160−161.
(36) Enz, U.; Fast, J. F.; van Houten, S.; Smit, J. *Philip Res. Reports* **1962**, *17*, 451−463.
(37) McGuire, T. R.; Argyle, B. E.; Shafer, M. W.; Smart, J. S. *J. Appl. Phys.* **1963**, *34(4)*, 1345−1346.
(38) Gorter, E. W. *J. Appl. Phys.* **1963**, *34(4)* 1253−1259.
(39) Frederikse, H. P. R. *CRC Handbook of Chemistry and Physics,* 78th ed.; CRC: New York, 1997; pp 12−118.

Figure 7. The reciprocal of the molar magnetic susceptibility of EuSe₂ versus temperature for both ZFC and FC data. (A) Measurements on a polycrystalline sample. (B) Measurements on single crystals, with the field parallel to the *c*-axis. The ZFC data are shown with open circles and FC data are displayed as x's. Both sets of data were fitted with a straight line from 50 to 300 K.

± 0.2, which is consistent with the theoretical value calculated for the Eu²⁺ free ion (7.94).[40] Although magnetization versus field curves at room temperature showed a linear dependence, at 5 K we observed significant departures from linearity (low field region) and saturation above 25 kG (see Figure 8). Magnetization loops within the field region of ±55 kG indicated an odd-shaped "hysteresis" loop characteristic of a metamagnetic transition (see Figure 8).

To probe further into the nature of this phenomenon, we decided to study the magnetic susceptibility and magnetization of single crystals along the various crystallographic directions. The reciprocal molar susceptibility at high temperatures (50 to 300 K) for the single crystals was in excellent agreement with powder samples and confirmed the observed μ_{eff} and Curie–Weiss behavior, see Figure 7B. We found a peak in the susceptibility at at $T_n = 8$ K (see Figure 9), when measured in the direction parallel to the *c*-axis, with no change between ZFC and FC measurements, which is consistent with antiferromagnetism. When measured in the direction parallel to the *a*-axis, we observed a much smaller susceptibility than along the *c*-axis, which

(40) Selwood, P. W. *Magnetochemistry,* Second Edition; Interscience: New York, 1956.
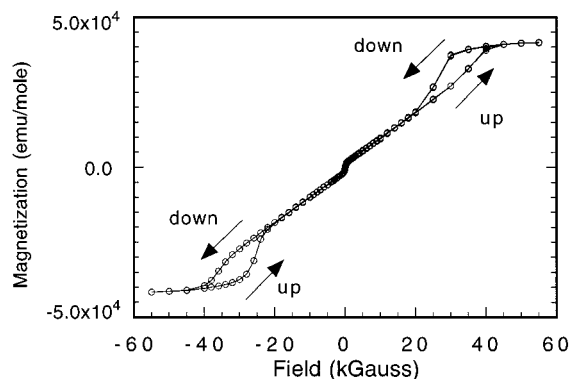
Figure 8. Field dependence of magnetization for a polycrystalline powder sample of EuSe$_2$ at 2.5 K, measured both in increasing and decreasing magnetic field.
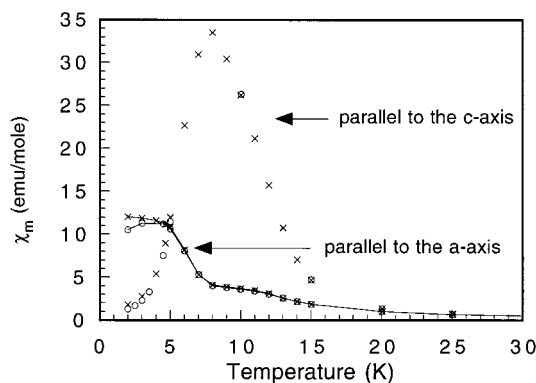
Figure 9. The molar magnetic susceptibility versus temperature for ZFC data and FC data parallel to both the *c*-axis and *a*-axis of single crystals of EuSe$_2$. The ZFC data measured parallel to the *c*-axis are shown with open circles and FC data are shown as x's. The ZFC data measured parallel to the *a*-axis are shown by circles with a line through them and FC data are represented by x's with a line through them. The bump in the ZFC and FC data parallel to the *a*-axis, in the region of 8−13 K, can be explained by the uncertainty in the exact orientations of the crystals on the rotor.

increased with falling temperature below T_n, reaching a constant value at about 4 K. It should be noted that the small bump in the ZFC and FC data in the region 8−13 K, when measured parallel to the *a*-axis can be explained by pointing out that we cannot be certain the crystals were mounted perfectly flat on the quartz plate and thus a difference as small as 5° would cause us to see some behavior from the *c-axis* direction. The magnetic susceptibility was also studied as a function of angle where the significant anisotropic character of EuSe$_2$ is readily apparent (see Figure 10). The field-dependent magnetization along the *c*-axis showed a metamagnetic transition near 20 kG that saturates at $M_s \approx 40\,000$ emu/mol, (see Figure 11). The magnetization along the *a*-axis is more or less linear up to 40 kG, but it too saturates at the same value. This result agrees, within experimental error, with the value 39 100 emu/mol calculated from

$$M_s = gSN\mu_B \qquad (2)$$

where g is 2, S is the total spin (here 7/2), N is Avogadro's number, and μ_B is the Bohr Magneton, which is equal to 9.27×10^{-21} erg/G. In addition, there was no observable hysteresis in any of the M(H) curves. In
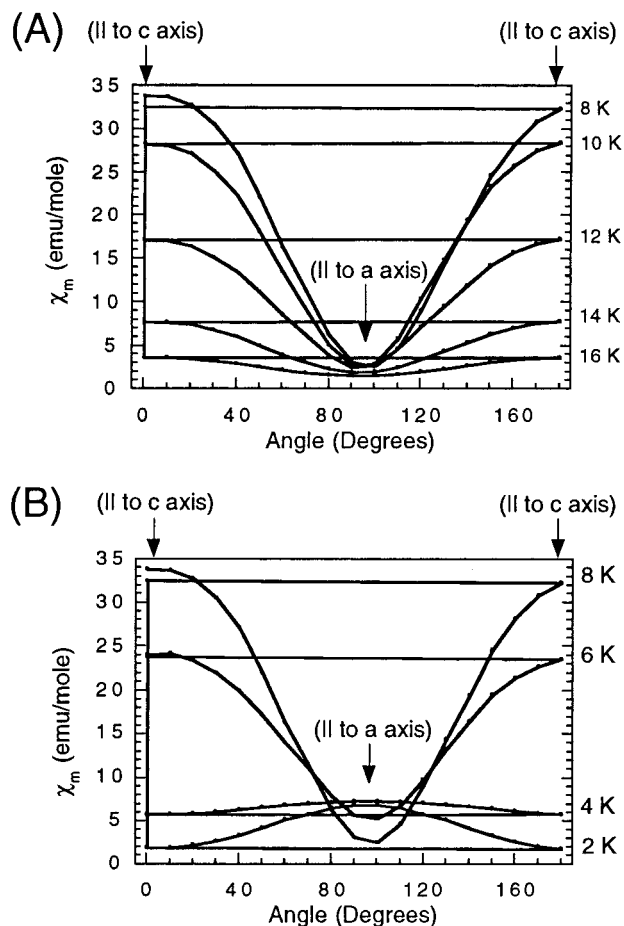
Figure 10. The molar magnetic susceptibility versus angle for single crystals of EuSe$_2$ at various temperatures. A significant amount of anisotropy can be seen when comparing the χ_m measured parallel and perpendicular to the *c*-axis: (A) the angle dependence in the temperature region 8−16 K; (B) the same dependence in the temperature region 2−8 K.
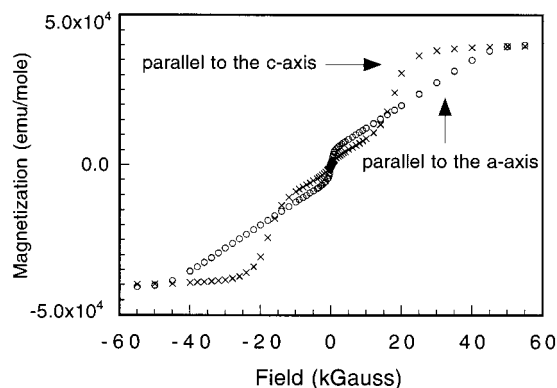
Figure 11. Field dependence of magnetization for EuSe$_2$ at 2.5 K measured both parallel to the *c*-axis (x) and parallel to the *a*-axis (open circles).

retrospect, the "hysteresis" loop observed in the powder data is actually due to the different magnetization of the material in the two different crystallographic directions.

Almost all of these results can be understood using a simple spin model where all Eu^{2+} spins in the *ab*-plane are coupled ferromagnetically with the magnetization parallel to the *c*-axis (see Figure 12A). Adjacent ferromagnetic sheets are then coupled antiferromagnetically to form a bulk antiferromagnet. In contrast to this spin

(A)

(B)

(C)

applied field
parallel to c-axis
20 kGauss

applied field
parallel to a-axis
40 kGauss
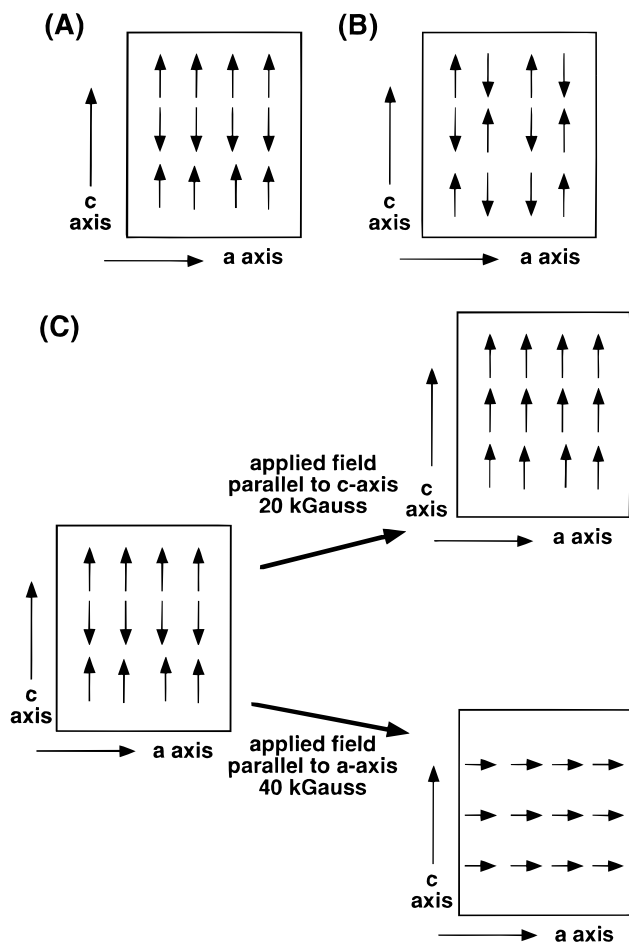
Figure 12. (A) Spin model for EuSe$_2$ in which adjacent ferromagnetic sheets in the ab-plane are coupled antiferromagnetically. (B) A typical antiferromagnet shown for comparison. (C) Field-induced spin flip in EuSe$_2$ associated with the metamagnetic transition. A field of 20 kG applied along the *c*-axis is needed to accomplish the transition.

model, a typical antiferromagnet is shown in Figure 12B. The application of 20 kG along the *c*-axis is sufficient to reverse the ferromagnetic sheets that point in the "wrong" direction, whereas a field of 40 kG in the *a*-axis direction tips both sublattices to saturation (see Figure 12C). These magnetic structures are consistent with the fact that the Eu−Se−Eu bond angles are 90° in the ab-plane, which generally favors ferromagnetism, whereas they are 76° and 140° in the ac-plane, which favors antiferromagnetism.[41] In addition, all Eu−Se bond lengths are 3.17 Å.

The small inflection point in the M(H) curves near 100 G (see Figure 11) is not so easily understood. In the model, the magnetization should be a linear function of magnetic field up to the critical field H_c. This feature could be associated with an initially facile canting of spins that later becomes more restricted prior to saturation at ~50 kG. In view of the lack of hysteresis, it is unlikely that this feature is due to a ferromagnetic impurity. Furthermore, there is no evidence of an impurity because hand-picked single crystals were used for these experiments and, when ground, the powder X-ray diffraction pattern of the crystals, performed after

magnetic measurements, can be indexed completely to EuSe$_2$ (although powder X-ray diffraction cannot detect impurites of less than ~1%). This small inflection point in the M(H) curves, therefore, must be an intrinsic property of the material.

Although a neutron diffraction study, which could verify the current model and provide further information to clarify these discrepancies, is possible, it may be prohibitive because of the high cost of Eu metal and its very large neutron capture cross-section.[42] The system, however, may be an excellent candidate for magnetic X-ray scattering, which requires significantly less sample and provides similar information.[43]

We have found in the literature that several, divalent Eu-containing compounds exhibit metamagnetic transitions, however, these compounds are very different from EuSe$_2$ because they are intermetallic.[44−46] Furthermore, the metamagnetic behavior was observed in powder samples, and no angle-dependent studies were conducted. No possible spin models were proposed to explain the observations in these studies. The present contribution provides a rare glimpse at the anisotropic nature of the metamagnetic phenomenon in Eu compounds, which is to be contrasted with the more or less isotropic behavior of ferromagnetic EuSe.

Concluding Remarks

EuSe$_2$ is a new rare-earth dichalcogenide accessible via alkali metal chalcogenide flux at 540 °C, which cannot be made from direct combination of the elements. EuSe$_2$ decomposes to EuSe at 569 °C. The structure is CuAl$_2$ type with rows of staggered diselenide dumbbells separated by Eu atoms. EuSe$_2$ is a semiconductor with a band gap of 1.43 eV. In contrast to ferromagnetic EuSe, EuSe$_2$ behaves as a bulk antiferromagnet with a metamagnetic transition below 8 K. The Eu^{2+} spins in the ab-plane seem to be coupled ferromagnetically to form a ferromagnetic sheet. It is an exceptional occurrence that a new binary compound will be found given the many decades of synthetic investigations. This, of course, underscores in a most definitive way the valuable contributions flux synthesis can make to the discovery of not only complex but also simple new materials.

(41) Anderson, P. W. *Magnetism*, Vol. 1; Rado, G. T.; Suhl, H., Eds.; Academic: New York, 1963; pp 25−85.

(42) Wilson, A. J. C. *International Tables of Crystallography*; Kluwer: Boston, 1995; p 388.
(43) Watson, D.; Nuttall, W. J.; Forgan, E. M.; Perry, S. C.; Fort, D. *Phys. Rev. B* **1998**, *57(14)* R8095−R8098.
(44) Katoh, K.; Takabatake, T.; Minami, A.; Oguro, I.; Sawa, H. *J. Alloys Compd.* **1997**, *261:(1−2)*, 32−36.
(45) Pöttgen, R. *J. Mater. Chem.* **1996**, *6(1)*, 63−67.
(46) Ernet, U.; Müllmann, R.; Mosel, B. D.; Eckert, H.; Pöttgen, R.; Kotzyba, G. *J. Mater. Chem.* **1997**, *7(2)*, 255−257.